Rapid thermalization by baryon injection in gauge/gravity duality

Koji Hashimoto,[1,*] Norihiro Iizuka,[2,†] and Takashi Oka[3,‡]

[1]*Mathematical Physics Lab., RIKEN Nishina Center, Saitama 351-0198, Japan*
[2]*Theory Division, CERN, CH-1211 Geneva 23, Switzerland*
[3]*Department of Physics, Faculty of Science, University of Tokyo, Tokyo 113-0033, Japan*

Using the AdS/CFT correspondence for strongly coupled gauge theories, we calculate thermalization of mesons caused by a time-dependent change of a baryon-number chemical potential. On the gravity side, the thermalization corresponds to a horizon formation on the probe flavor brane in the AdS throat. Since heavy-ion collisions are locally approximated by a sudden change of the baryon-number chemical potential, we discuss the implication of our results to RHIC and LHC experiments, to find a rough estimate of the rather rapid thermalization time-scale $t_{\rm th} < 1$ [fm/c]. We also discuss the universality of our analysis against varying gauge theories.

I. INTRODUCTION

The AdS/CFT correspondence [1–3], or more broadly, the gauge/gravity duality, is an extremely useful tool to study strongly coupled field theories. Recently, this correspondence has been applied to various field theory settings, and these applications open up many new correspondences between gravity and other branches of physics. Perhaps one of the most surprising things in the success of using gravity to study strongly coupled gauge theories is that it seems to work even for an explanation of heavy-ion collision experiment data at Brookhaven's Relativistic Heavy Ion Collider (RHIC). In RHIC experiments [4,5], one of the big surprises was that a quark-gluon plasma (QGP) forms at a very early stage [6] just after the heavy-ion collision, i.e., a rapid thermalization occurs. This obviously requires a theoretical explanation, but remains as a challenge, because this requires a calculation of the strongly coupled field theory in the nonequilibrium process. In this paper, we study the thermalization in strongly coupled field theories by using the gauge/gravity duality.

The key idea is to approximate the heavy-ion collision by a sudden change of a baryon-number chemical potential locally at the collision point. Using the AdS/CFT correspondence, we obtain strongly coupled gauge theory calculations for the thermalization, where a time-dependent confinement/deconfinement transition occurs due to a sudden change of the baryon-number chemical potential, with dynamical degrees of freedom changing from mesons to quark/gluon thermal plasma. We calculate a time scale for that. Our strategy can be summarized briefly as follows: on the gravity side of the AdS/CFT correspondence, the change in the baryon chemical potential is encoded in how we throw in the baryonically charged fundamental

strings (F strings) from the boundary to the bulk. Since the F-string endpoint is a source term for the gauge fields on the flavor brane in the AdS bulk, this provides a time-dependent gauge field configuration. This induces a time-dependent effective metric for the degrees of freedom on the flavor brane, which are mesons. As a result, this yields the emergence of an apparent horizon on the flavor brane, which signals, in the dual strongly coupled field theory, the "thermalization of mesons," by which we mean that the meson degrees of freedom change into quark and gluon degrees of freedom with thermal equilibrium.

Any computation of thermalization of mesons due to the injection of the baryon charge in strongly coupled gauge theories has never been proposed. We provide a generic framework for it in this paper. We also present computations at different gauge theories, and argue how universal the thermalization time-scale is. We also discuss its implication in strongly coupled gauge theories, which hopefully offers a path to realistic QCD. The observation of the flavor thermalization due to changes of external parameters (i.e., quantum quench) different from the baryon charge, was studied in [7]. Previous studies on holographic thermalization, for example, [8–12] discussed glueball sectors, while ours observes the meson sector thermalization. What we see is the thermalization on the probe flavor brane. Since the back-reaction is not taken in our setting, this thermalization is not at all related to the one of the glueball sectors.

In our framework, the only input is the function which represents how we throw in the baryonically charged F-strings. Therefore, we have a small number of parameters, which includes a typical maximum value of the baryon density and the time scale for changing the chemical potential. With collision parameters at RHIC, we obtain the thermalization time-scale as $t_{\rm th} < 1$ [fm/c]. Actually, this time scale can be well compared with the known hydrodynamic simulation requirement $t_{\rm th} < 2$ [fm/c] discussed, for example, in [13–17]. We also "predict" that

*koji(at)riken.jp
†norihiro.iizuka(at)cern.ch
‡oka(at)cms.phys.s.u-tokyo.ac.jp

heavy-ion collisions at LHC exhibit slightly smaller order of the time scale for thermalization as $t_{th} \lesssim \mathcal{O}(0.1)$ [fm/c].

Let us make a few more comments about comparing our analysis with the data. As we mentioned previously, we are discussing the time scale of "thermalization of mesons," which is the horizon formation on the probe brane only. In real-world experiments, such as RHIC or LHC, thermalization should involve not only mesons but also glueballs, which corresponds to the black hole horizon formation in the bulk geometry, not only on the probe brane. Since we are not treating the glueball sectors, the "prediction" above in order to compare our analysis with the data is unfortunately not as accurate as it should be. Another problem for comparison with data is that we are discussing the large N limit of gauge theories. Therefore, the reader should regard our analysis as just an indication of rapid thermalization of some sectors of the large N gauge theories.

In the following, after solving the equations in the gravity side with a generic time-dependent baryon chemical potential, we compute the apparent horizon and the time scale for the thermalization. The simplest example offered is $\mathcal{N} = 4$ super Yang-Mills with $\mathcal{N} = 2$ hypermultiplets as "quarks." We conclude with the statement of the universality, by showing some variations of the setup, including quark masses and confining scales.

II. D3-D7 SYSTEM WITH QUARK INJECTION

The simplest setup in AdS/CFT with quarks is the $\mathcal{N} = 2$ supersymmetric massless QCD constructed by a D3-D7 system [18], where we consider the gravity back-reaction of only D3-branes and regard D7-brane as a prove flavor brane. We are interested in the dynamics of mesons and the deconfinement of quarks, which is totally encoded in the probe flavor D7-brane in the $AdS_5 \times S^5$ geometry,

$$ds^2 = \frac{r^2}{R^2} \eta_{\mu\nu} dx^\mu dx^\nu + \frac{R^2}{r^2}(d\rho^2 + \rho^2 d\Omega_3^2 + dw_5^2 + dw_6^2),$$ (1)

where $\rho^2 \equiv w_1^2 + w_2^2 + w_3^2 + w_4^2$ and $r^2 \equiv \rho^2 + w_5^2 + w_6^2$. R is the AdS radius defined by $R^4 = 4\pi g_s N_c \alpha'^2$. The string coupling is related to the QCD coupling as $2\pi g_s \equiv g_{QCD}^2$. The dynamics of the flavor D7-brane is determined by the D7-brane action

$$S = -\mu_7 \int d^8\xi \sqrt{-\det(G_{ab} + 2\pi\alpha' F_{ab})},$$ (2)

where the D7-brane is at $w_5 = 0$, and are extended on the gauge theory directions x^μ ($\mu = 0, 1, 2, 3$), ρ, and Ω^3. The fluctuations of gauge fields A_a (or, scalar field $\eta \equiv w_6$) on the D7-brane corresponds to vector (or, scalar)

mesons. For a concise review of the D3-D7 system and meson dynamics, see [19]. G_{ab} is the induced metric on the D7-brane. The asymptotic ($\rho \rightarrow \infty$) value of η corresponds to the quark mass $m_q = \eta/2\pi\alpha'$. For simplicity, we first put it at zero. This corresponding to a "marginal confinement" for the mesons on the flavor brane since it has only zero-sized horizon [20]. The D7-brane tension is $\mu_7 \equiv 1/(2\pi)^7 g_s \alpha'^4$.

In AdS/CFT, the response to the change in the baryon chemical potential is totally encoded in this D7-brane action. We will solve this gauge field for the arbitrary time-dependent chemical potential.

As the chemical potential of our interest is homogeneous, we may turn on only the F_{tr} component. With a redefinition of the AdS radial coordinate $z \equiv R^2/\rho$, the D7-brane action (2) is equivalent to a $1 + 1$-dimensional Born-Infeld system in a curved background,

$$S = -\mu_7 V_3 \text{Vol}(S^3) \int dt dz \frac{R^8}{z^5} \sqrt{1 - \frac{z^4}{R^4}(2\pi\alpha')^2 F_{tz}^2}, \quad (3)$$

where V_3 is the volume of $x^{1,2,3}$ space.

In the AdS/CFT dictionary, the static baryon chemical potential corresponds to $A_t(r = \infty) - A_t(r = 0)$. This basically counts the number of electric charges located at the origin $r = 0$. In order to change this number in a time-dependent manner, we need to consider an additional source term

$$\delta S = \mu_7 V_3 \text{Vol}(S^3) \int dt dz (A_t j^t + A_z j^z), \quad (4)$$

which describes the end points of a fundamental string (electric charges) thrown in from the outside of the system, i.e., from the boundary into the bulk. See Fig. 1. Since the geodesic of the fundamental string end-points is the light geodesics determined by the induced metric G_{ab}, and in the present case $G_{tt} = -G_{zz}$, it is just along a null vector $(v_t, v_z) = (1, -1)$. Therefore, the source current is an arbitrary function of the variable $t - z$. With a current conservation relation, we obtain that $j^t = j^z$, and we take the arbitrary source function as $j^t = j^z = g'(t - z)$. Given this source current j, the gauge field strength F_{tz} is readily solved from the equations of motion on the D7-brane and we obtain

$$(2\pi\alpha') F_{tz} = \frac{R^2 z g(t - z)}{\sqrt{(2\pi\alpha')^2 R^{12} + z^6 (g(t - z))^2}}. \quad (5)$$

This is the gauge field solution which encodes the information of the time-dependent chemical potential given the source current $j^t = j^z = g'(t - z)$.

The relation between g and the chemical potential is linear. For the static case $g(t - z) = $ constant, the solution (5) is nothing but a conventional Born-Infeld solution on a D-brane. So we can compare the Born-Infeld charge g with
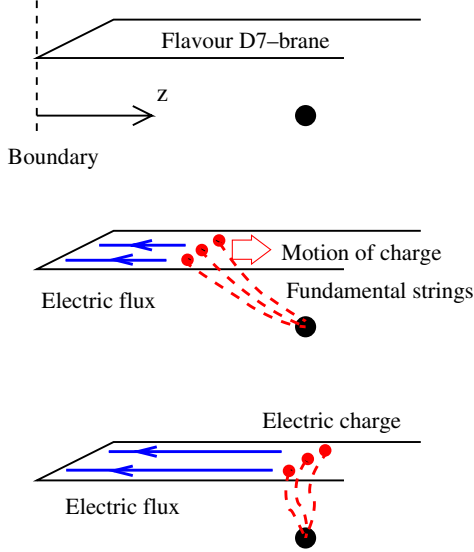
FIG. 1 (color online). How the baryon charge density changes in time, as we throw-in fundamental strings from the boundary. Top figure: there is no baryon charge. Bottom figure: the static baryon (quark) charge is provided by the fundamental strings (dashed lines) connecting the probe D7-brane and the AdS horizon (black blob). The end points of the fundamental strings are electric charges (flavor charges) on the D7-brane. An electric flux (solid lines with arrows) emanates from those charges on the D7-brane. Middle figure: the flavor electric charges are thrown-in from the AdS boundary into the bulk. This specifies the time-dependent chemical potential. The electric flux is time-dependent. The big arrow denotes the motion of the electric charges on the D7-brane.

the fundamental string charge (which equals the quark number), following the techniques found in [21], to obtain

$$g(t) = (2/\pi)(2\pi\alpha')^4 \lambda n_{\mathrm{B}}(t), \qquad (6)$$

where the baryon-number density is $n_B = n_{\mathrm{quark}}/N_c$ at the boundary $z = 0$. This determines the normalization of the baryon number, in the solution (5) of the D7-brane system.

III. HORIZON FORMATION ON THE FLAVOR D7-BRANE

A time-dependent configuration on the D7-brane modifies the effective metric which the fluctuations on the D7-brane feel. A large field configuration creates a horizon of the metric on the D7-brane, which signals the thermalization in AdS/CFT. From the induced metric with the background gauge configuration (5), here we compute the location of an apparent horizon on the D7-brane [22].

Let us compute an effective metric which a scalar fluctuation η feels, which is massless scalar meson-like pion field. By expanding the D7-brane action (2) for small fluctuation $\delta\eta$ in the background solution F_{tz} (5) to the quadratic order, we can obtain effective metric $\tilde{g}$ as:

$$S = -\int dt dz d^3 x^i d^3 \theta^I \frac{\sqrt{-\tilde{g}}}{2} \tilde{g}^{MN} \partial_M \delta\eta \partial_N \delta\eta + \mathcal{O}(\delta\eta^3), \qquad (7)$$

where $i = 1, 2, 3$ are the spatial directions of our $3 + 1$-dimensional space-time, and θ^I ($I = 1, 2, 3$) is the angular variable on the S^3. (M, N) shows the whole $7 + 1$ directions on D7-branes, (t, z, i, I). The effective metric $\tilde{g}$ can be obtained easily,

$$-\tilde{g}_{tt} = \tilde{g}_{zz} = \mu_7^{1/3} R^{4/3} z^{-4/3} (1 - z^4 R^{-4} (2\pi\alpha'^2) F_{tz}^2)^{5/6},$$

$$\tilde{g}_{ij} = \mu_7^{1/3} R^{4/3} z^{-4/3} (1 - z^4 R^{-4} (2\pi\alpha'^2) F_{tz}^2)^{-1/6} \delta_{ij},$$

$$\tilde{g}_{IJ} = \mu_7^{1/3} R^{4/3} z^{2/3} (1 - z^4 R^{-4} (2\pi\alpha'^2) F_{tz}^2)^{-1/6} G_{IJ}, \qquad (8)$$

where G_{IJ} is the metric on the unit 3-sphere.

Given this effective metric, we will now determine the apparent horizon, which is defined locally as a surface whose area variation vanishes along the null rays which are normal to the surface. The surface area at an arbitrary point in given (t, z) is

$$V_{\mathrm{surface}} = \int d^3 x^i d^3 \theta^I \sqrt{(\Pi_{i=1,2,3}\tilde{g}_{ii})(\Pi_{I=1,2,3}\tilde{g}_{II})}$$

$$= V_3 \mathrm{Vol}(S^3) \mu_7 R^4 z^{-1} (1 - z^4 R^{-4} (2\pi\alpha'^2) F_{tz}^2)^{-1/2}. \qquad (9)$$

The (t, z) space-time has a trivial null vector normal to the surface $(v^t, v^z) = (1, -1)$ since $\tilde{g}_{zz} = -\tilde{g}_{tt}$, so the constancy of the surface area variation along this null ray is

$$dV_{\mathrm{surface}}|_{dt=-dz} = 0, \qquad (10)$$

which yields

$$(\partial_z - \partial_t)[z^2 (1 - z^4 R^{-4} (2\pi\alpha'^2) F_{tz}^2)] = 0. \qquad (11)$$

Substituting the gauge field solution (5) to this, we obtain the following equation

$$(2\pi\alpha')^2 R^{12} - 2z^6 g^2 + 2z^7 g g' = 0. \qquad (12)$$

If this Eq. (12) admits a solution, it specifies where the apparent horizon on the D7-brane is formed.

Before we proceed, a few comments are in order. First, we are calculating the apparent horizon, not the event horizon on the flavor brane. Since apparent horizon is always inside the event horizon, as long as apparent horizon never disappears at finite time, we can regard the formation of the apparent horizon as a signal of the thermalization of system. However since the positions of the apparent horizon are time-dependent, it is difficult to extrapolate the thermodynamical information, such as temperature, which is determined by the event horizon. On the other hand, the apparent horizons are defined locally without knowing the late time asymptotics, therefore it has a calculation simplicity. Second, we are using the Born-Infeld action on the flavor D7-brane to determine the

effective metric for the various mesonic modes. This Born-Infeld form is crucial, since if we had used the Yang-Mills form for the D7's degrees of freedom, the horizon would have not formed. The reason why we need the Born-Infeld form is due to the warping in the (1), which makes the effective string tension α' finite, so it is not appropriate to replace the Born-Infeld action by the simple Yang-Mills form.

IV. THERMALIZATION TIME-SCALE ORDER ESTIMATION

From (12), we can order-estimate the thermalization time-scale by a dimensional analysis without specifying the explicit form of the source function $g(t - z)$. We would like to consider the chemical potential change which mimics the heavy-ion collisions. The function $g(t - z)$ at the AdS$_5$ boundary $z = 0$ is directly related to the time-dependent baryon number according to (6) as $g(t) = (2/\pi)(2\pi\alpha')^4 \lambda n_B(t)$.

Suppose that $g(t - z)$ changes like trigonometric functions from zero to some maximal value during the time scale $1/w$. This is like the situation where the chemical potential change locally by two baryonically charged heavy ions approaching each other. Setting the maximal value of $g(t - z)$ as g_{max}, we can order-estimate it as

$$g(\xi) \sim g_{max}, \qquad g'(\xi) \sim w g_{max}. \qquad (13)$$

Then, a dimensional analysis of (12) estimates the thermalization time-scale t_{th} as

$$t_{th} \sim \left(\frac{(2\pi\alpha')^2 R^{12}}{g_{max}^2}\right)^{1/6} \sim \left(\frac{\lambda}{n_B^2}\right)^{1/6}, \qquad (14)$$

if $t_{th}w \lesssim 1$ is satisfied. Here n_B being the maximal baryon-number density determined as $g_{max} = 4(2\pi\alpha')^4 \lambda n_B$. If $t_{th}w \gg 1$ instead, then we obtain,

$$t_{th} \sim \left(\frac{(2\pi\alpha')^2 R^{12}}{g_{max}^2 w}\right)^{1/7} \sim \left(\frac{\lambda}{n_B^2 w}\right)^{1/7}. \qquad (15)$$

On the other hand, if $g(\xi)$ has an explicit ξ dependence like a power-law behavior to approach its maximum, such as $g(\xi) \propto \xi^n$, with positive n, then

$$g(\xi) \sim g_{max}(w\xi)^n, \qquad g'(\xi) \sim w g_{max}(w\xi)^{n-1}. \qquad (16)$$

Again, a dimensional analysis yields,

$$t_{th} \sim \left(\frac{(2\pi\alpha')^2 R^{12}}{g_{max}^2 w^{2n}}\right)^{1/(6+2n)} \sim \left(\frac{\lambda}{n_B^2 w^{2n}}\right)^{1/(6+2n)}. \qquad (17)$$

In summary, in terms of following parameters, inverse of the variation time scale of the baryon chemical potential w, 't Hooft coupling λ, and the maximum baryon density n_B, the thermalization time-scale is written as

$$t_{th} \sim \left(\frac{\lambda}{n_B^2 w^k}\right)^{1/(6+k)} \qquad (18)$$

for given $k(\geq 0)$, which is determined by how we change the baryon-number chemical potential. This is one of our main results.

In the following, we present two explicit examples of the source function $g(\xi)$ and show that both examples exhibit the generic behavior (18). The first example is for a baryonic matter formation, and the second is for baryons colliding and passing through each other.

V. EXAMPLE I: BARYONIC MATTER FORMATION

To understand the time scale in more detail, let us investigate a few explicit examples. The first example presented here mimics colliding baryons forming a baryonic matter. We start with zero baryon density $n_B = 0$ and then increase it linearly in time, for $0 < t < 1/w$. It reaches the maximum at $t = 1/w$ and then it is kept constant. This is like two baryonically charged heavy-ion approaching each other, followed by a formation of a QGP gas with large baryon number. Setting $\xi \equiv t - z$, we arrange the function g accordingly as

$$g(\xi) = \begin{cases} 0 & (\xi < 0) \\ g_{max} w \xi & (0 < \xi < 1/w) \\ g_{max} & (1/w < \xi) \end{cases} \qquad (19)$$

With this choice of the time-dependent baryon-number density, we can compute the location of the apparent horizon from (12). The results are,

$$t = \frac{3z}{2} + \frac{1}{2}\sqrt{z^2 + \frac{\lambda}{z^6(2\pi)^4 n_B^2 w^2}} \quad \text{(for } t < z + 1/w\text{)}, \qquad (20)$$

and

$$z = \frac{1}{2\pi^{2/3}}\left(\frac{\lambda}{n_B^2}\right)^{1/6} \quad \text{(for } t > z + 1/w\text{)}. \qquad (21)$$
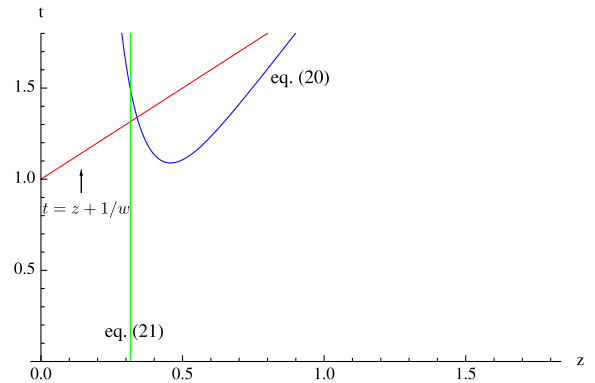

FIG. 2 (color online). Locations of the apparent horizon in z-t plane written in the unit of $1/w$ for the parameter is chosen such that $(\lambda/(2\pi n_B^2))^{1/6} = 1/w$.

The curve (20) crosses with line $t = z + 1/w$ at $z = z_0$, where z_0 satisfies

$$1 - z_0 w - \frac{\lambda}{64\pi^4 n_B^2 z_0^6} = 0, \qquad (22)$$

and in the case $z_0 w \ll 1$, $z = z_0$ coincides with the curve (21). These results are shown in Fig. 2.

The slight discontinuity between curves (20) and (21) is simply due to a cusp of the input source function (19) at $\xi = 1/w$. If we smooth the source function (19), then the two curves (20) and (21) are connected smoothly. Just for a comparison, in Fig. 3 we also show the location curve for the apparent horizon for a smooth source current given by

$$g(\xi) = g_{\max} \frac{1}{2}(1 + \tanh(2w\xi - 1))$$

$$= \begin{cases} 0 & (w\xi \ll 1/2) \\ g_{\max} w\xi & (w\xi \sim 1/2) \\ g_{\max} & (w\xi \gg 1/2) \end{cases} \qquad (23)$$

Figure 3 is well compared with Fig. 2.

The emergence of the horizon on the flavor D7-brane is seen by the boundary observer through a light propagation on the D7-brane. Suppose that the point A at (t_A, z_A) in Fig. 4 gives the earliest delivery of the information of the apparent horizon. Because the light geodesic toward the AdS$_5$ boundary is again along the null vector $(v^t, v^z) = (1, -1)$, it is clear that the point A is determined by the curve (20) and its tangential outgoing null line, and it gives

$$t_A = c_{At}(\lambda/n_B^2 w^2)^{1/8}, \qquad z_A = c_{Az}(\lambda/n_B^2 w^2)^{1/8}, \quad (24)$$
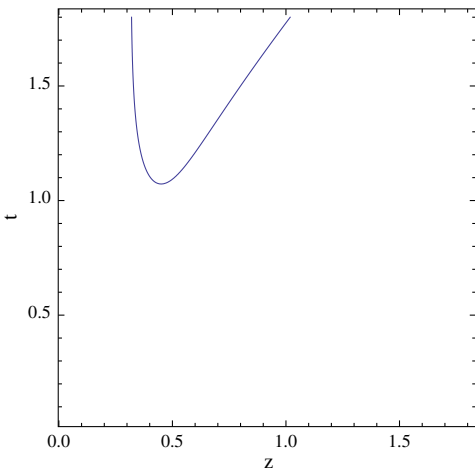

FIG. 3 (color online).   A numerical solution for the location of the apparent horizon for the source current given by $g(\xi)$ of (23), where the parameters and the unit are the same as Fig. 2. This is a smoothened version of the curve analytically determined in Fig. 2.
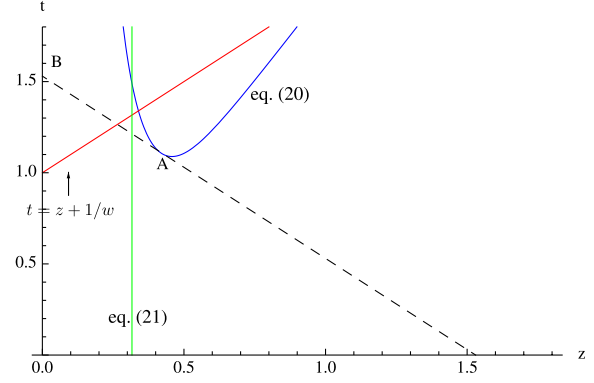

FIG. 4 (color online).   Earliest thermalization for the boundary observer occurs at point A, which is the tangential point between curve (20) and the light ray propagating toward boundary (dashed line). The boundary observer see the thermalization at point B. We choose the same parameter as Fig. 2.

where c_{At} and c_{Az} are order-one coefficients and given by $c_{At} \equiv (11\sqrt{73} - 13)^{1/2}/(48(2\pi)^4(5\sqrt{73} - 31)^3)^{1/8} \approx 0.88$ and $c_{Az} \equiv ((5\sqrt{73} - 31)/48(2\pi)^4)^{1/8} \approx 0.33$. As a result, the thermalization time seen by the boundary observer is

$$t_{\rm th} = t_A + z_A = (c_{At} + c_{Az})\left(\frac{\lambda}{n_B^2 w^2}\right)^{1/8} \sim \left(\frac{\lambda}{n_B^2 w^2}\right)^{1/8}. \quad (25)$$

On the other hand, it is also possible that the point C in Fig. 5 gives the earliest occasion, depending on the values of the parameters in the source function $g(\xi)$. This happens especially if

$$\frac{1}{w} \ll \left(\frac{\lambda}{n_B^2 w^2}\right)^{1/8}. \qquad (26)$$

In this case, similarly, we can compute the thermalization time $t_{\rm th}$ as
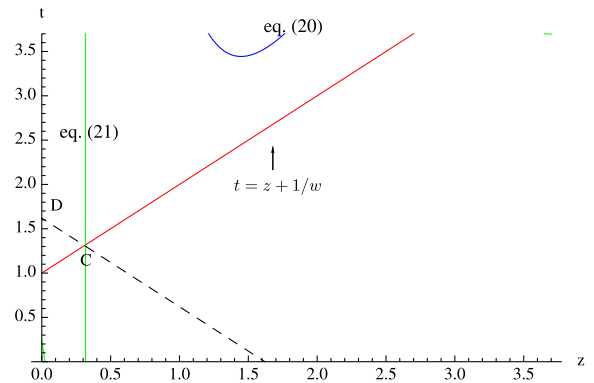

FIG. 5 (color online).   Curves for the parameter chosen $(\lambda/(2\pi n_B^2))^{1/6} = (10)^{2/3}/w$, written in the unit of $1/w$. Thermalization occurs at point C, which is the crossing point between line (21) and the line $t = z + 1/w$. From point C, the light ray is propagating toward boundary (black line), and the boundary observer see the thermalization at point D.

$$t_{\rm th} = t_C + z_C, \qquad (27)$$

with

$$t_C = \frac{1}{w} + z_C, \qquad z_C \equiv \frac{1}{2\pi^{2/3}}\left(\frac{\lambda}{n_B^2}\right)^{1/6}, \qquad (28)$$

where z_C is given by the line (21). Therefore,

$$t_{\rm th} = 2z_C + \frac{1}{w} = \frac{1}{\pi^{2/3}}\left(\frac{\lambda}{n_B^2}\right)^{1/6} + \frac{1}{w}. \qquad (29)$$

Because of the inequality (26), $1/w \ll 2z_C$, this yields

$$t_{\rm th} \sim \left(\frac{\lambda}{n_B^2}\right)^{1/6}. \qquad (30)$$

These results (25) and (30) are consistent with the order estimation (18) in the previous section.

VI. EXAMPLE II: BARYONS PASSING THROUGH EACH OTHER

Let us investigate another explicit example. This second example mimics baryons which first collide with each other, then pass each other, and then leave. We start with zero baryon density $n_B = 0$ and then increase it linearly in time, for $0 < t < 1/w$. It reaches the maximum at $t = 1/w$ and then decrease to zero again. This is like two baryonically charged heavy-ion approaching each other, and then they pass by due to the asymptotic freedom. Setting $\xi \equiv t - z$, we arrange the function g accordingly as

$$g(\xi) = \begin{cases} 0 & (\xi < 0) \\ g_{\rm max} w\xi & (0 < \xi < 1/w) \\ g_{\rm max}(2 - w\xi) & (1/w < \xi < 2/w) \\ 0 & (2/w < \xi) \end{cases}, \qquad (31)$$
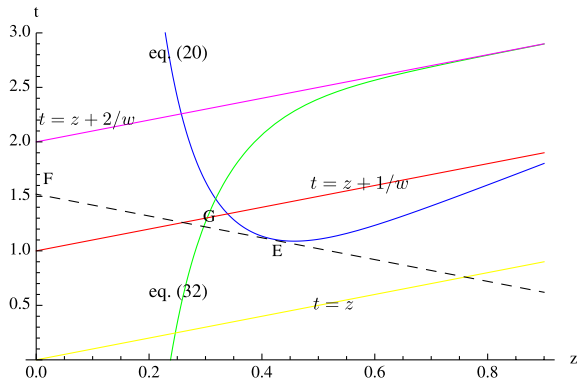

FIG. 6 (color online).   The curves (20) and (32) and $t = z$, $t = z + 1/w$, $t = z + 2/w$, and light ray (dashed) toward boundary which is tangential to (20) in the unit of $1/w$, where the parameter is chosen such that $(\lambda/(2\pi n_B^2))^{1/6} = 1/w$. It is clear from this parameter that the earliest apparent horizon is seen at point F, which is similar to point B in Fig. 4.

where $g_{\rm max} \equiv (2/\pi)(2\pi\alpha')^4 \lambda n_B$ with n_B is the maximum baryon-number density. Compared with an explicit example I, the location of the apparent horizon for $0 < \xi < 1/w$ is again given by the curve (20). On the other hand, for $1/w < \xi < 2/w$, the curve is given by

$$t = \frac{2}{w} + \frac{3z}{2} - \frac{1}{2}\sqrt{z^2 + \frac{\lambda}{z^6(2\pi)^4 n_B^2 w^2}} \qquad (32)$$

(for $z + 1/w < t < z + 2/w$).

Finally, for $z + 2/w < t$, (12) admits no solution, which means that there is no apparent horizon in this region. In Fig. 6, we plot these curves in the z-t plane.

Similarly, for a comparison, in Fig. 7, we show also the location curve for the apparent horizon for a smooth source which takes a Gaussian form as

$$g(\xi) = g_{\rm max}\exp(-(2w)^2(\xi - 1/w)^2). \qquad (33)$$

Figure 7 is well compared with Fig. 6.

Similar to the explicit example I, from the curves (20) and (32), we can derive the thermalization time $t_{\rm th}$. From (20), we obtain again (25). The thermalization point (32) is at the crossing of the lines in Fig. 6. The z value of this crossing point, written as z_G, is a solution of the equation

$$\frac{z_G^7}{w} + \frac{z_G^6}{w^2} - \frac{\lambda}{4(2\pi)^4 n_B^2 w^2} = 0. \qquad (34)$$

With this, the thermalization time from the curve (32) is computed as $t_{\rm th} = 2z_G + 1/w$. Therefore, from the two curves, we obtain the thermalization time as the earliest occasion among these two,
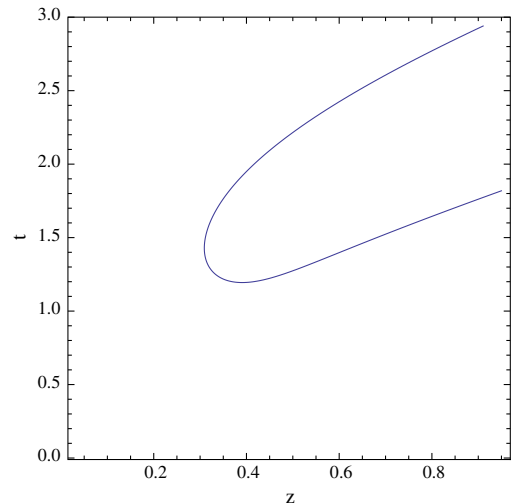

FIG. 7 (color online).   A numerical solution for the location of the apparent horizon written in the unit of $1/w$ for the source current which is given by $g(\xi)$ of (33), where the parameters are chosen as $(\lambda/(2\pi n_B^2))^{1/6} = 1/w$ and written in the unit of $1/w$. This is a smoothened version of the curve analytically determined in Fig. 6.

$$t_{\text{th}} = \min\left\{ (c_{At} + c_{Az})\left(\frac{\lambda}{n_B^2 w^2}\right)^{1/8}, 2z_G + \frac{1}{w} \right\}. \quad (35)$$

Note that in the case where the first term and the third term are well balanced in Eq. (34), it gives,

$$z_G \sim \left(\frac{\lambda}{n_B^2 w}\right)^{1/7}. \quad (36)$$

On the other hand, if the second term and the third term are balanced in Eq. (34),

$$z_G \sim \left(\frac{\lambda}{n_B^2}\right)^{1/6}. \quad (37)$$

Therefore, if

$$1/w \lesssim t_{\text{th}} \quad (38)$$

is satisfied, thermalization time-scale (35) becomes the lowest scale

$$t_{\text{th}} \sim \min_{\{k=0,1,2\}}\left\{ \left(\frac{\lambda}{n_B^2 w^k}\right)^{1/(6+k)} \right\}. \quad (39)$$

Again, this is consistent with the generic order estimation (18).

VII. COMPARISON WITH EXPERIMENTS

We will later discuss the validity and the universality of our results in various other theories which are QCD-like theories. But before that, it is quite entertaining to substitute realistic values of the parameters and compare our results with the data, even though our setting is not realistic QCD at this point. For RHIC and LHC heavy-ion collisions, the baryons are passing through each other, so we may approximate them by the example II above [23].

First, let us consider RHIC parameters. It is natural to assume that n_B is twice the standard nuclear density n_N times the Lorentz contraction factor γ, i.e., $n_B \sim 2\gamma n_N$, where $n_N \sim 0.17$ [fm]$^{-3}$. In RHIC experiments, we have heavy-ion Au-Au collisions with $A = 197$. The Lorentz factor is given by the ratio between its energy scale $E = \sqrt{s_{NN}}/2 \sim 100$ [GeV] and the mass of Au m_{Au}, therefore $\gamma = E/m_{\text{Au}} \sim 100$. On the other hand, at RHIC, the time scale $1/w$ should be given by the time scale of two nuclei passing by through their bodies, where two nuclei are propagating almost with the velocity of light. Therefore, $1/w$ is well approximated as $1/w \sim 2A^{1/3}/\gamma$ [fm/c], where A is the nucleon number and $2A^{1/3}$ [fm] is the typical nuclear diameter. This gives $1/w \sim 0.1$ [fm/c].

With these inputs at hand, we obtain

$$\left(\frac{\lambda}{w^2 n_B^2}\right)^{1/8} \sim \left(\frac{A^{2/3}\lambda}{\gamma^4 n_N^2}\right)^{1/8} \sim 0.24 \times \lambda^{1/8} \text{ [fm/c]}. \quad (40)$$

Similarly,

$$\left(\frac{\lambda}{wn_B^2}\right)^{1/7} \sim \left(\frac{A^{1/3}\lambda}{\gamma^3 n_N^2}\right)^{1/7} \sim 0.30 \times \lambda^{1/7} \text{ [fm/c]}, \quad (41)$$

$$\left(\frac{\lambda}{n_B^2}\right)^{1/6} \sim \left(\frac{\lambda}{\gamma^2 n_N^2}\right)^{1/6} \sim 0.39 \times \lambda^{1/6} \text{ [fm/c]}. \quad (42)$$

These are all bigger than $1/w \sim 0.1$, therefore, approximately (38) is satisfied. In gauge/gravity duality, the 'tHooft coupling $\lambda = g_{\text{QCD}}^2 N_c$ is taken to be very large. However, *since the power of λ in t_{th} is small (less than one), t_{th} can not take a large value, even for large λ.* Actually, we use $\lambda \sim \mathcal{O}(10)$ which is often used in gauge/gravity duality for the spectrum comparison. In this case, the smallest of these are given by (40), though all the scales (40)–(42) give the same order time scale. Therefore, we obtain the thermalization time-scale as

$$t_{\text{th}} < 1 \text{ [fm/c]}. \quad (43)$$

It is interesting that this time scale can be well compared with the known hydrodynamic simulation requirement $t_{\text{th}} < 2$ [fm/c] [13–17]. We found a rather rapid thermalization of mesons.

Our calculation can also gives a prediction for heavy-ion collisions at LHC. In LHC where Pb-Pb ion collision experiments are ongoing, the energy scale is bigger than RHIC as $\sqrt{s_{NN}} = 2.7$ TeV [24]. The Lorentz factor is $\gamma = E/m_{\text{Pb}} \sim 1000$, due to the center of mass difference, and therefore, γ is 10 times bigger in LHC than RHIC. Since $A \approx 200$ is almost the same, these give $1/w \sim 0.01$ [fm/c]. With these at hand, we can compute the thermalization time-scale. Because of the difference of Lorentz factor γ compared with RHIC case in (40)–(42), the thermalization time-scale is suppressed furthermore in LHC, and we obtain

$$t_{\text{th}} \lesssim \mathcal{O}(0.1) \text{ [fm/c]}. \quad (44)$$

Again, with $\lambda \sim \mathcal{O}(10)$ is used. (Because of the asymptotic freedom, $\lambda_{\text{LHC}} < \lambda_{\text{RHIC}}$, however, the difference between $\lambda_{\text{RHIC}} < \lambda_{\text{LHC}}$ is tiny, therefore, we can neglect this effect..) This (44) gives a significantly faster thermalization time-scale compared to RHIC.

VIII. THERMALIZATION FOR VARIOUS MODES

Given the calculation of the scalar meson thermalization in the massless $\mathcal{N} = 2$ supersymmetric QCD, it is straightforward to extend the calculation of the thermalization for other degrees of freedom.

First, instead of the thermalization of the scalar meson η, let us consider that of vector mesons A_M. A similar computation leads to an effective metric of A_M on the D7-brane, which gives the equation for the apparent horizon as

$$(\partial_z - \partial_t)[z^4(1 - z^4 R^{-4}(2\pi\alpha'^2)F_{tz}^2)] = 0. \quad (45)$$

This differs from (11) by just a power in the z factor. According to this modification, the thermalization time is just $2^{1/3}$ times that of the scalar meson. Therefore, the thermalization time-scale (43) is almost common in order, for various vector meson excitations on the flavor branes.

Next, we consider effects of the quark mass. The quark mass m_q corresponds to the boundary location of the D7-brane, $\eta(z=0) = 2\pi\alpha' m_q$. This shifts the D7-brane a bit. One can compute the full effect of this shift in our formalism, but we can give a naive estimate as follows. Noticing the fact that η comes in the effective metric always as a combination $(R^2/z^2 + \eta^2/R^2)$ instead of just R^2/z^2, our computation presented here for $\eta = 0$ is valid when

$$R^2/z^2 \gg \eta^2/R^2. \qquad (46)$$

Substituting the expression of z by z_C given by (28), we obtain

$$m_q \ll (\sqrt{2}\lambda n_B/\pi)^{1/3}. \qquad (47)$$

Even without relying on the large 'tHooft coupling limit, this is generally satisfied for three light flavors, for the standard nuclear density. Therefore, again we expect that the thermalization time-scale (43) is almost common in order, even for the various meson excitations with different flavors, such as up, down, and strange.

IX. DISCUSSION ON UNIVERSALITY AND REAL-WORLD QCD

We saw that either in massless or massive $\mathcal{N} = 2$ supersymmetric QCD, the calculations of the thermalization time-scales of the various meson modes are always given by (18). Given this, it is natural to ask to what extent our thermalization time-scale (18) holds for a larger variety of gauge theories. Since this question is related to a possible universality and also to real-world QCD-related problems, we shall discuss this question now.

First, note that even though our setting admits supersymmetry, it is also clear that we have never used the fermion properties for our thermalization calculations. Therefore, we expect that our results are not very dependent on the supersymmetry.

Next, we shall see that even with different background metrics, our thermalization time-scale (18) is universal. We have used the AdS$_5$ metric (1), which represents the deconfined phase for the gluon sectors in the conformal $\mathcal{N} = 4$ theory. However, the conformality of the gluon sector in the metric (1) is not important at all since our computations of thermalization reply only on the asymptotic part ($z < z_0$) of the induced metric, where z_0 is the point where the apparent horizon emerges (such as z_A, z_C, z_E, z_G in our explicit examples I and II). Therefore, we claim that our results hold for other theories where IR dynamics of gluons are significantly different from our

theory. Even if we replace the metric (1) by some other nonconformal metric which does not admit a bulk horizon, such as a cutoff AdS$_5$ at $z \gtrsim z_0$, due to the fact that our calculations are insensitive to the IR regime of the geometry at $z \gtrsim z_0$, our conclusion is still valid. In this sense, we expect that our thermalization time-scale (18) is not only for the $\mathcal{N} = 2$ theory, but rather it works for a broader category of nonconformal theories.

The scale $z_0 \lesssim O(1)$ [fm] in the example I and II we studied corresponds to the energy scale $\gtrsim \mathcal{O}(200)$ [MeV]. Therefore, for any nonconformal theory which admits confinement/deconfinement transition for the gluon sectors at the scale smaller than 200 [MeV], our result (43) for the thermalization of mesons is expected to be valid. For the real-world QCD, confinement/deconfinement transition is ~200 [MeV], which is the validity bound of our analysis, therefore, it is expected that our results (43) also hold even for realistic QCD. However, to confirm this, further study is necessary.

Let us discuss confining gauge theories a bit more. On the gravity side, confinement is implemented as a deformation at the IR region ($z \sim \infty$) of the geometry. If we use successful hard-wall models in the bottom-up models of holographic QCD, which has a cutoff of AdS$_5$ at IR $z > z_0$, then we obtain the same thermalization time-scale. One other example is a confining geometry made by D3-$D(-1)$ system [25,26], which has the AdS$_5$ form at the UV region. In the solution, the $D(-1)$s (D-instantons) condense in the bulk and back-react to modify the IR $r \rightarrow 0$ region by emitting the dilaton ϕ as

$$ds^2 = e^{\phi/2} \times (\text{AdS}_5 \times S^5 \text{geometry}), \quad e^\phi = 1 + \frac{q}{r^4}. \qquad (48)$$

Here, ds^2 is the metric in the string frame. In the UV $r \rightarrow \infty$, this reduces to the AdS metric (1), as advertised. The $D(-1)$ charge q (which is proportional to QCD instanton charge density) is related to the QCD string tension τ_{QCD}, as $q/R^8 = \pi^2 \lambda^{-1} \tau_{\text{QCD}}^2$. This breaks the supersymmetries by half. The universality is valid if this factor e^ϕ may not significantly modify the asymptotic geometry around $z < z_0$, therefore, we need to require $q < R^8 z_0^{-4}$. With (28), this translates to a condition

$$\tau_{\text{QCD}} < 2^{5/3} \lambda^{1/6} n_B^{2/3}. \qquad (49)$$

Realistic parameters used in this paper show that τ_{QCD} is at a comparable order with the right-hand side, so this effect may modify the thermalization time-scale only slightly by an $\mathcal{O}(1)$ factor. Further study would be interesting for these.

Finally, we comment on possible generalization of our approach for future works. We have conducted the calculations with the abelian Born-Infeld action, which treat a single flavor brane. In order to treat multiflavors, we need to extend our analysis to nonabelian Born-Infeld action. It is interesting to generalize our study to nonabelian flavor

branes and study the flavor dependence of the thermalization time-scale. Since our thermalization calculations are insensitive to the IR but are sensitive to the UV regime, if we consider totally different bulk geometries which do not approach the AdS_5 metric (1), our result (18) is no longer valid. It is quite interesting to generalize our approach to other theories where their UV geometries are different from ours, such as the holographic QCD model by D4-D8 on Witten's geometry [27,28], or Lifshitz type of geometries [29] for an application to condensed matter systems. We leave these studies for future works.

[1] J. M. Maldacena, Adv. Theor. Math. Phys. **2**, 231 (1998); Int. J. Theor. Phys. **38**, 1113 (1999).

[2] S. S. Gubser, I. R. Klebanov, and A. M. Polyakov, Phys. Lett. B **428**, 105 (1998).

[3] E. Witten, Adv. Theor. Math. Phys. **2**, 253 (1998).

[4] E. Shuryak, Prog. Part. Nucl. Phys. **53**, 273 (2004).

[5] E. V. Shuryak, Nucl. Phys. **A750**, 64 (2005).

[6] U. W. Heinz, AIP Conf. Proc. **739**, 163 (2004).

[7] S. R. Das, T. Nishioka, and T. Takayanagi, J. High Energy Phys. 07 (2010) 071.

[8] R. A. Janik and R. B. Peschanski, Phys. Rev. D **74**, 046007 (2006).

[9] P. M. Chesler and L. G. Yaffe, Phys. Rev. Lett. **102**, 211601 (2009).

[10] S. Bhattacharyya and S. Minwalla, J. High Energy Phys. 09 (2009) 034.

[11] P. M. Chesler and L. G. Yaffe, Phys. Rev. D **82**, 026006 (2010).

[12] P. M. Chesler and L. G. Yaffe, Phys. Rev. Lett. **106**, 021601 (2011).

[13] P. F. Kolb, P. Huovinen, U. W. Heinz, and H. Heiselberg, Phys. Lett. B **500**, 232 (2001).

[14] T. Hirano, Phys. Rev. C **65**, 011901 (2001).

[15] P. Huovinen, arXiv:nucl-th/0108033.

[16] D. Teaney, J. Lauret, and E. V. Shuryak, arXiv:nucl-th/0110037.

[17] U. W. Heinz and P. F. Kolb, *The 18th Winter Workshop on Nuclear Dynamics*, edited by W. Bauer, *et al.* [Heavy Ion Physics (to be published)].

[18] A. Karch and E. Katz, J. High Energy Phys. 06 (2002) 043.

[19] J. Erdmenger, N. Evans, I. Kirsch, and E. Threlfall, Eur. Phys. J. A **35**, 81 (2008).

[20] Therefore, this D7-brane is already touching the zero size (and zero temperature) bulk horizon, which is so-called "black hole embedding." Note that this induces zero temperature black hole on the probe D7-brane, which indicates "marginally confining phase" because of zero temperature. However in this paper, we analyze how the *nonzero size* (and nonzero temperature) horizon is formed on this probe brane due to the time-dependent chemical potential change.

[21] C. G. Callan and J. M. Maldacena, Nucl. Phys. **B513**, 198 (1998).

[22] It is a difficult issue to define a temperature in a time-dependent system. Since an event horizon is always outside of the apparent horizon, as far as apparent horizons do not disappear, we regard the emergence of an apparent horizon as a signal of thermalization. Event horizons cannot be defined locally, while apparent horizons can. In static space-time, these two horizons coincide.

[23] Our calculations just treat homogeneous change of the baryon chemical potential. However, in heavy-ion collisions, various momentum effects should take place. So, our estimate presented here should be regarded as just an order-estimate.

[24] T. A. Collaboration, Phys. Rev. Lett. **105**, 252303 (2010).

[25] H. Liu and A. A. Tseytlin, Nucl. Phys. **B553**, 231 (1999).

[26] A. Kehagias and K. Sfetsos, Phys. Lett. B **456**, 22 (1999).

[27] E. Witten, Adv. Theor. Math. Phys. **2**, 505 (1998).

[28] T. Sakai and S. Sugimoto, Prog. Theor. Phys. **113**, 843 (2005).

[29] S. Kachru, X. Liu, and M. Mulligan, Phys. Rev. D **78**, 106005 (2008).